Direct detection of a transport-blocking trap in a nanoscaled silicon single-electron transistor by radio-frequency reflectometry

B. J. Villis, A. O. Orlov, S. Barraud, M. Vinet, M. Sanquer, P. Fay, G. Snider, and X. Jehl

Citation: Applied Physics Letters 104, 233503 (2014); doi: 10.1063/1.4883228

View online: http://dx.doi.org/10.1063/1.4883228

View Table of Contents: http://scitation.aip.org/content/aip/journal/apl/104/23?ver=pdfcov

Published by the AIP Publishing

Articles you may be interested in

Defect detection in nano-scale transistors based on radio-frequency reflectometry Appl. Phys. Lett. **99**, 152106 (2011); 10.1063/1.3647555

Experimental study on quantum confinement effects in silicon nanowire metal-oxide-semiconductor field-effect transistors and single-electron transistors

J. Appl. Phys. **103**, 053709 (2008); 10.1063/1.2874247

Coulomb blockade oscillations in ultrathin gate oxide silicon single-electron transistors

J. Appl. Phys. **97**, 116106 (2005); 10.1063/1.1921335

Single-shot readout with the radio-frequency single-electron transistor in the presence of charge noise Appl. Phys. Lett. **86**, 143117 (2005); 10.1063/1.1897423

Charge noise analysis of an AlGaAs/GaAs quantum dot using transmission-type radio-frequency single-electron transistor technique

Appl. Phys. Lett. 77, 543 (2000); 10.1063/1.127038





Direct detection of a transport-blocking trap in a nanoscaled silicon single-electron transistor by radio-frequency reflectometry

B. J. Villis, $^{1,2,a)}$ A. O. Orlov, 1,2,3 S. Barraud, 1,4 M. Vinet, 1,4 M. Sanquer, 1,2 P. Fay, 3 G. Snider, and X. Jehl 1,2

¹Université Grenoble Alpes, INAC-SPSMS, F-38000 Grenoble, France

(Received 2 May 2014; accepted 26 May 2014; published online 11 June 2014)

The continuous downscaling of transistors results in nanoscale devices which require fewer and fewer charged carriers for their operation. The ultimate charge controlled device, the single-electron transistor (SET), controls the transfer of individual electrons. It is also the most sensitive electrometer, and as a result the electron transport through it can be dramatically affected by nearby charges. Standard direct-current characterization techniques, however, are often unable to unambiguously detect and resolve the origin of the observed changes in SET behavior arising from changes in the charge state of a capacitively coupled trap. Using a radio-frequency (RF) reflectometry technique, we are able to unequivocally detect this process, in very close agreement with modeling of the trap's occupation probability. © 2014 AIP Publishing LLC. [http://dx.doi.org/10.1063/1.4883228]

The ability of a single-electron transistor (SET) to detect very small charge variations enables a uniquely precise way of characterizing complementary metal-oxide-semiconductor (CMOS) relevant materials (e.g., gate stacks containing novel dielectrics). Over the past decade, a method for charged defect detection in nanowire transistors was established, 1-3 based on measurement of SET low frequency (LF) differential conductance $G = dI/dV_{ds}$ for slowly changing gate (V_g) and source-drain (V_{ds}) voltages. In this way, the stability plots of $G(V_g, V_{ds})$, "Coulomb diamond plots," are obtained. If charged defects (traps) are present near the SET island, charging processes in the SET-trap system affect the electron transport through the SET due to electrostatic interactions between the SET and the trap. As a result, the observed Coulomb diamond pattern strongly deviates from the ideal model. By considering charging processes in a SET-trap system, represented by a network of capacitors and tunnel junctions, one can very accurately map the distortions in the experimentally measured diamonds to the simulations with just a few adjustable parameters. This technique provides a means for precise identification of traps near the SET island (e.g., in the tunnel barriers).^{3,4} However, it is not sensitive to any charging events occurring in the regions of the diamond plot where the SET main island electron population, n_m , is constant, because in these regions no directcurrent (DC) is flowing through the SET. For example, if trap population, n_t changes, while n_m stays constant, it cannot be detected by the LF conductance technique because the current is blocked.

An alternative tool to investigate charging mechanisms in the SET coupled to charged defects is RF reflectometry. In this technique, transitions in the charge states cause variations in the RF signals (either reflected or transmitted).

Cheong *et al.*⁵ investigated the RF impedance of an AlGaAs/GaAs SET with two individually adjustable tunnel junctions and demonstrated the ability to detect single electron charging through a single tunnel junction. This technique was also recently applied for charge detection in a metal oxide single-electron box⁶ and used to detect single-electron charging in a capacitively coupled polycrystalline Si nanowire.⁷

In this paper, we demonstrate the detection of a trap that blocks transport through the SET using RF reflectometry. In particular, we observe the trap population change within the Coulomb blockaded region, where SET conductance is completely suppressed.

The experimental setup is based on that described in Refs. 7 and 8 where a single phase homodyne detector was used for carrier signal demodulation. The source electrode of the SET is grounded and the drain is connected to a 150 nH inductor that (along with a parasitic capacitor to ground of approximately 0.3 pF) forms a tank circuit resonating at 782 MHz. Under the experimental conditions used here (i.e., very large resistance of tunnel junctions) the SET is strongly overcoupled to the feedline and impedance matching conditions cannot be fulfilled. Therefore, the benefit of using a tank circuit comes primarily from its frequency and phase sensitivity near the resonant frequency. The LF differential conductance is obtained by a standard 2-wire measurement with a lock-in detector through the DC port of the bias tee.

In the reported experiment, the signal of interest corresponds to a weak modulation of RF reflection in response to changes in the (DC) gate voltage. To obtain the highest sensitivity for this signal, we acquired the derivative of the reflection coefficient, $d\Gamma/dV_g$ implemented by superimposing a small modulating signal ($f_M \approx 430\,\mathrm{kHz}$) on the DC gate voltage. As a result, the reflected carrier signal at the drain is amplitude modulated at a frequency f_M . After demodulating this reflected signal to baseband using

²CEA, INAC-SPSMS, F-38000 Grenoble, France

³Department of Electrical Engineering, University of Notre Dame, Notre Dame, Indiana 46556, USA

⁴CEA, LETI, Minatec campus, F-38054 Grenoble, France

a) Now at the London Centre for Nanotechnology, University College London, London WC1H 0AH, United Kingdom.

homodyne detection with a mixer, the sideband at f_M arising from the gate modulation is further amplified and rectified with an RF lock-in amplifier; the effective bandwidth of the recovered signal is ≈ 0.25 Hz. To determine the effective complex admittance of the device, as recently demonstrated by several groups 10-13 simultaneous acquisition of amplitude and phase of the demodulated signal is required. The use of homodyne detection as presented here limits our detection capabilities to the changes in signal amplitude. Therefore, for the data shown here, the phase of the local oscillator for the homodyne demodulation was adjusted to maximize the signal from the drain-coupled trap under investigation. As we will show below, the trap charging process in our case is similar to a charging process in a single-electron box, coupled to the drain of the SET. Under this condition, the features in the demodulated signal that correspond to the Coulomb diamonds, predominantly defined by the SET conductance, are strongly suppressed.

The sample studied here is a Si MOS-SET similar to those used in Ref. 1, with lithographically defined dimensions of the Si island: $80\,\mathrm{nm}$ wide, $17\,\mathrm{nm}$ thick, and $50\,\mathrm{nm}$ long. The island is separated from a polycrystalline Si gate by a $10\,\mathrm{nm}$ SiO₂ gate oxide. Coulomb blockade dominates electron transport at temperatures below approximately $10\,\mathrm{K}$.

The LF measurement of G is shown in Fig. 1(a) as a map of V_{ds} and V_g measured at T=800 mK. This measurement reveals strong deviations from the regularly shaped

Coulomb diamond pattern, namely, a distorted sawtooth pattern along the conductance edge of the diamond at finite bias with an abnormally large region of suppressed conductance appearing as two overlapped diamonds, and two narrow regions of negative differential conductance (NDC), marked in red. Since the NDC lines have positive slope, they correspond to the charge exchange occurring in the drain-island area.³ Therefore, we hypothesized that it is likely that a single trap located near the SET drain (e.g., an As donor located under the spacer), may be responsible for the observed features. Magnetic field spectroscopy has been used previously to measure the spin of single-charge traps with the Zeeman splitting. To have a strong effect on the SET conductance such a trap must be tunnel coupled to the SET island and the drain, and capacitively coupled to the gate, forming a network shown in Fig. 1(c).

We solve the steady state solution ($\hat{\Gamma} \mathbf{P} = 0$) of the master equation for the vector \mathbf{P} of probabilities of discrete charge states of the island: $\frac{\partial \mathbf{P}}{\partial t} = \hat{\Gamma} \mathbf{P}$ using the technique described in Refs. 1–3. The matrix $\hat{\Gamma}$ contains the transition rates for sequential tunneling through all four tunnel junctions of the circuit. The system is treated in the metallic limit; therefore, the rates are obtained from the tunnel Hamiltonian using Fermi's golden rule. The result of this simulation is shown in Fig. 1(b). A very good agreement between the simulation and measurement is obtained. The capacitance values used in the simulations, $C_g = 12$ aF and $C_d = C_s = 8$ aF, were chosen to

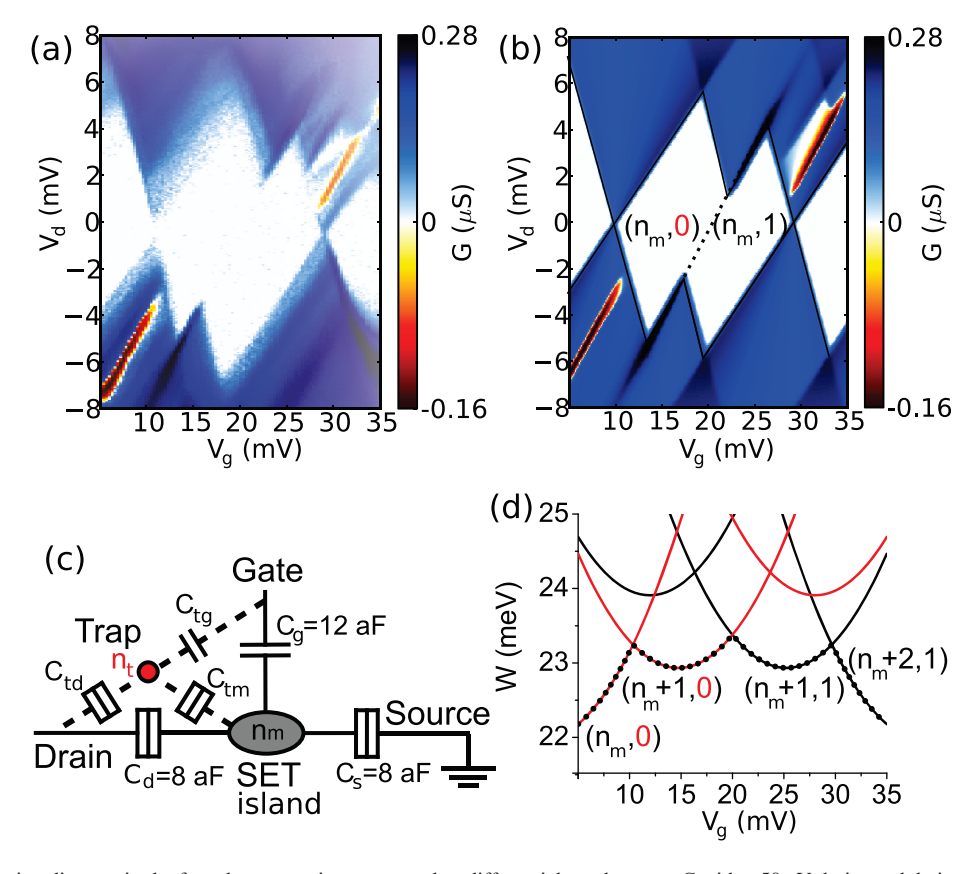


FIG. 1. (a) The charging diagram in the few electron regime measured as differential conductance G with a 50 μ V drain modulation at 77.1 Hz. (b) Simulation of G using the capacitance network between SET main island and trap shown in (c). (c) Capacitances and tunnel conductances used for best agreement with the experimental data. The negative differential conductance features require an asymmetry between $G_{td} = 0.05 \frac{e^2}{h}$ and $G_{tm} = 0.0007 \frac{e^2}{h}$. (d) Energy of the charge states at zero V_{ds} bias as a function of V_g . The different charge states are specified by (n_m, n_t) , where n_m and n_t are the SET island and trap occupation, respectively. The red (black) parabolas are for an empty (full) trap. The dotted line indicates the ground state of the whole system (SET and trap).

match the period and charging energy of the Coulomb diamonds in Fig. 1(a). The coupling between the SET and trap was then chosen to match the perturbed Coulomb diamonds in Fig. 1(a) using the relationship^{1,2}

$$\alpha_t = \frac{C_{tg}}{C_{\Sigma t}} = 0.18; \quad \beta_t = \frac{C_{tm}}{C_{\Sigma t}} = 0.45,$$

where $C_{\Sigma t} = C_{td} + C_{tg} + C_{tm}$ is the total capacitance of the trap and the other capacitances are as defined in Fig. 1(c). The specific values of α_t and β_t suggest that the trap has a slightly stronger capacitive coupling to the SET island than to the drain electrode. To obtain agreement between the simulation in Fig. 1(b) and measurement in Fig. 1(a), particularly in the conducting regions, there is no need for an asymmetry in the resistance of the barriers between the SET island and the drain and source. Consequently, we have used the same values, indicated in the legend of Fig. 1(c). In contrast, an asymmetry in the tunnel resistances between the trap and the drain/SET island is required to achieve a good match with the experiment (specifically, $G_{td} = 0.05 \frac{e^2}{h}$ between trap and drain and $G_{tm} = 0.0007 \frac{e^2}{h}$, between trap and SET island). A lower value of R_{td} enhances the NDC features, while a lower R_{tm} softens them. This suggests that the trap is located closer to the drain contact than to the SET island, which may, for example, correspond to an implanted dopant located beneath the drain spacer.² The electrostatic model of a single charge trap tunnel coupled to the SET can be understood by considering the energy levels of the different charge states of the system, defined by

$$W(n_{m}, n_{t}) = \frac{e^{2} \left(n_{m} + \beta_{t} n_{t} - \frac{C_{d} V_{ds} + C_{g} V_{g}}{e}\right)^{2}}{2(C_{\Sigma m} + \beta_{t} C_{\Sigma t})} + \frac{e^{2} \left(n_{t} - \frac{C_{td} V_{ds} + C_{tg} V_{g}}{e}\right)^{2}}{2C_{\Sigma t}}.$$

Here, $C_{\Sigma t}$ is assumed to be relatively small (1.4 aF here) so that the total capacitance of the SET island is given by $C_{\Sigma m} = C_d + C_s + C_g = 28$ aF. In Fig. 1(d), the energy levels are shown at zero drain bias as a function of V_g using the capacitive coupling in Fig. 1(c). The dotted line corresponds to the ground state of the system. The intersection of the parabolas at approximately $V_g = 10\,\mathrm{mV}$ and 30 mV represent the degeneracy points of the SET island. The intersecting parabolas at $V_g = 20\,\mathrm{mV}$ represent the degeneracy point of the trap, i.e., a change in the trap occupation. The simulation of the occupation probabilities of the SET island and trap are shown, respectively, in Figs. 2(a) and 2(b). Over the entire

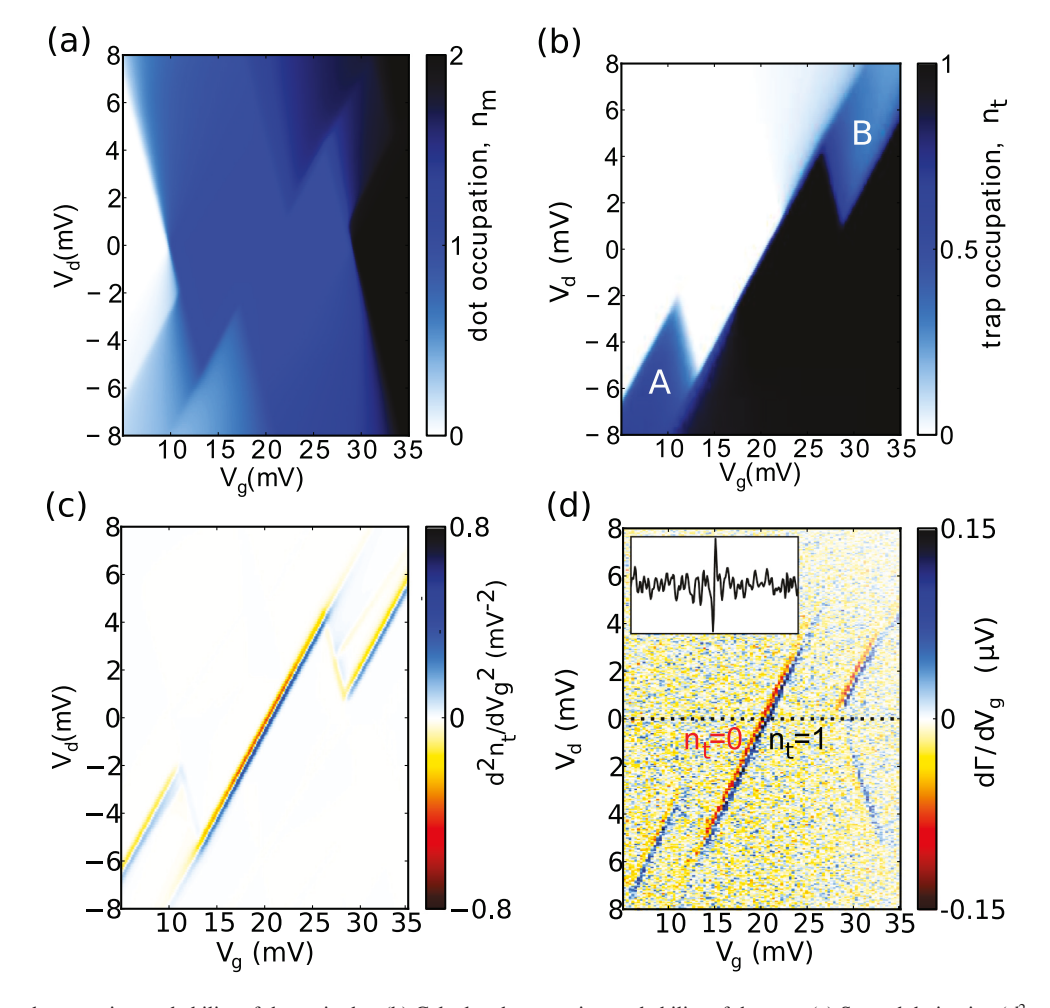


FIG. 2. (a) Calculated occupation probability of the main dot. (b) Calculated occupation probability of the trap. (c) Second derivative (d^2n_t/dV_g^2) of the calculated trap's population shown in b. (d) The corresponding RF reflected signal $d\Gamma/dV_g$ measured over the same region as shown in (a), (b), and (c) with a carrier RMS value of 5.5 μ V and a gate modulation of 0.2 mV. The inset of (d) shows the cross section of the dashed line at $V_{ds} = 0$ in the main figure.

range of the plot, the SET island occupation varies from 0 to 2, with a fixed value of 1 within the central blockaded region. It is in this region that the trap occupation, n_t , changes from 0 to 1 (see Fig. 2(b)). No direct source-drain current is associated with this process, hence this change in trap occupation is not directly detectable in a LF conductance measurement. Moreover, the charging of the trap leads to the enhancement of Coulomb blockade, strongly suppressing carrier transport through the SET. Nonetheless, the trap population change modulates the reflected RF signal by generating a small, capacitively coupled load on the tank circuit. Since the frequency of the RF excitation is higher than the tunneling rate Γ for trap charging $(2\pi f) = \frac{kT}{e^2R} \approx 300 \, \text{MHz}$), the power dissipated in the process saturates at its maximal level, thus improving the signal to noise ratio. ¹¹

A map of $d\Gamma/dV_g$ signal is shown in Fig. 2(d). Since this is a second derivative of an oscillatory signal, a change in charge state corresponds to a coupled (peak-dip) pair of lines (delineated by red/blue).⁷ Three such "paired lines" with a positive slope (dV_{ds}/dV_g) are clearly visible in experimental data Fig. 2(d). By applying the same technique as in Ref. 7, we calculated the second derivative of trap population, d^2n_t/dV_g^2 , shown in Fig. 2(c). This derivative, which resembles our measured signal, also shows coupled pairs of lines. As expected in our model, the charge exchange between drain and trap $(n_i: 0 \leftrightarrow 1)$ blocks the current flow through the SET.¹

At $V_g = 20$ mV, $V_{ds} = 0$ this transition corresponds to the system following the ground state as illustrated in Fig. 1(d), with no fractional trap population, leading to blockaded state with negligibly small differential conductance (Fig. 1(a)). At non-zero drain bias the model predicts two regions, labeled A and B, respectively, where the blockade is partially lifted and charge redistribution between SET island and trap occurs leading to a fractional trap population ($n_t = 0.5$, see Fig. 2(b)). These charge transitions (i.e., n_t : $0 \leftrightarrow 0.5$, and n_t : $0.5 \leftrightarrow 1$) manifest themselves as two paired lines at finite drain bias located left and right of the center line, also experimentally observed in Fig. 2(d). In LF measurement, these transitions are visible as two NDC lines, indicated by a red color in Figs. 1(a) and 1(b). There, a charge exchange

between the trap and the drain occurs, leading to an additional electrostatic repulsion for the electrons trying to tunnel in and out the SET island.

The application of RF reflectometry-based single-electron spectroscopy enables investigation of the charging processes that cannot be detected with traditional LF single electron spectroscopy. In this paper, we report the direct observation of charging of a trap located near the drain that blocks transport through the SET and show consistency with theoretical predictions.

We thank R. Wacquez and B. Previtali from CEA/LETI for sample fabrication and Benoît Roche for advice and assistance on simulations. Alexei Orlov acknowledges support from INAC and university Grenoble Alpes. Patrick Fay and Alexei Orlov acknowledge support from NSF Grant No. DMR-1207394. We also acknowledge the financial support from the EC FP7 FET-proactive NanoICT under Project SiAM No. 610637.

¹M. Hofheinz, X. Jehl, M. Sanquer, G. Molas, M. Vinet, and S. Deleonibus, Eur. Phys. J. B **54**, 299 (2006).

²M. Pierre, M. Hofheinz, X. Jehl, M. Sanquer, G. Molas, M. Vinet, and S. Deleonibus, Eur. Phys. J. B **70**, 475 (2009).

³H. C. George, M. Pierre, X. Jehl, A. O. Orlov, M. Sanquer, and G. L. Snider, Appl. Phys. Lett. **96**, 042114 (2010).

⁴V. N. Golovach, X. Jehl, M. Houzet, M. Pierre, B. Roche, M. Sanquer, and L. I. Glazman, Phys. Rev. B **83**, 075401 (2011).

⁵H. D. Cheong, T. Fujisawa, T. Hayashi, Y. Hirayama, and Y. H. Jeong, Appl. Phys. Lett. 81, 3257 (2002).

⁶F. Persson, C. Wilson, M. Sandberg, G. Johansson, and P. Delsing, Nano Lett. 10, 953 (2010).

⁷B. J. Villis, A. O. Orlov, X. Jehl, G. L. Snider, P. Fay, and M. Sanquer, Appl. Phys. Lett. **99**, 152106 (2011).

⁸Y. Tang, A. O. Orlov, G. L. Snider, and P. J. Fay, Appl. Phys. Lett. **95**, 193109 (2009).

⁹L. Roschier, P. Hakonen, K. Bladh, P. Delsing, K. W. Lehnert, L. Spietz, and R. J. Schoelkopf, J. Appl. Phys. 95, 1274 (2004).

¹⁰K. D. Petersson, C. G. Smith, D. Anderson, P. Atkinson, G. A. C. Jones, and D. A. Ritchie, Nano Lett. 10, 2789 (2010).

¹¹C. Ciccarelli and A. J. Ferguson, New J. Phys. **13**, 093015 (2011).

¹²S. J. Chorley, J. Wabnig, Z. V. Penfold-Fitch, K. D. Petersson, J. Frake, C. G. Smith, and M. R. Buitelaar, Phys. Rev. Lett. **108**, 036802 (2012).

¹³J. I. Colless, A. C. Mahoney, J. M. Hornibrook, A. C. Doherty, H. Lu, A. C. Gossard, and D. J. Reilly, Phys. Rev. Lett. 110, 046805 (2013).